ResearchGate

See discussions, stats, and author profiles for this publication at: https://www.researchgate.net/publication/231644891

Morphology, Structural Control, and Magnetic Properties of Carbon-Coated Nanoscaled NiRu Alloys

ARTICLE *in* THE JOURNAL OF PHYSICAL CHEMISTRY C · MAY 2010

Impact Factor: 4.77 · DOI: 10.1021/jp101965x

CITATIONS
18

READS
24

6 AUTHORS, INCLUDING:

Vyacheslav Khavrus
Technische Universität Dresden
44 PUBLICATIONS **385** CITATIONS
SEE PROFILE

A. Leonhardt
Leibniz Institute for Solid State and Materia…
185 PUBLICATIONS **3,321** CITATIONS
SEE PROFILE

Bernd Büchner
Leibniz Institute for Solid State and Materia…
1,043 PUBLICATIONS **15,144** CITATIONS
SEE PROFILE

Available from: Vyacheslav Khavrus
Retrieved on: 31 January 2016

Morphology, Structural Control, and Magnetic Properties of Carbon-Coated Nanoscaled NiRu Alloys

Ahmed A. El-Gendy,* Vyacheslav O. Khavrus, S. Hampel, A. Leonhardt, B. Büchner, and R. Klingeler

Leibniz Institute for Solid State and Materials Research (IFW), P.O. Box 270016, D-01171 Dresden, Germany

Received: March 4, 2010; Revised Manuscript Received: May 11, 2010

Carbon-coated nanoparticles of NiRu (NiRu@C) have been synthesized by a high-pressure chemical vapor deposition using metallocenes of both metals. Transmission electron microscopy images show an average particle size (core) of 8 ± 3 nm and carbon shell thicknesses between 2 and 3 nm. X-ray diffraction investigation reveals NiRu binary alloys. Analyses of the X-ray diffraction peaks and the magnetization curves approximately confirm the average particle size. The compositions of the nanoalloy cores have been studied by means of energy dispersive X-ray analysis. We find that at constant sublimation temperature (95 °C) a synthesis temperature of 900 °C and a Ni−Ru-metallocene weight ratio of 2:1, an increase of synthesis pressure leads to both a change of the core composition and the thickness of the carbon coatings. The magnetic properties of the coated nanoalloys strongly depend on the synthesis parameters so that, for example, the superparamagnetic blocking temperature and the saturation magnetization can be tailored. Our straightforward of controlled synthesis therefore opens a novel route to complex nanosized functional materials.

1. Introduction

Recently, core/shell nanoparticles are finding widespread applications since they combine the functionality of a core material with a protective coating, that is, the outer shell. In examples, the core/shell structure can enhance the thermal and chemical stability of the nanoparticles, can render them less cytotoxic, or might allow conjugation of other molecules to these particles. The shell can also prevent the oxidation of the core material.[1] However, possible defects of the shells might affect the shielding effect.[2,3] In addition, appropriate shells inhibit or at least deplete agglomeration of the particles so that the dispersity of the particles is improved. Because of the potential for applications, there are currently great efforts for synthesizing tailored core/shell nanostructures. In particular, the technology for the production of carbon-coated metal nanoparticles was developed fairly recently, and at present several different synthesis methods are applied. All these methods are however not yet fully understood so that further research and optimization is needed.[4]

Magnetic encapsulates are of particular interest in the field of tailoring novel nanomaterials since they may find applications in various branches of the high tech-industry, for example, in magnetic data storage, nanomedicine, electronics, magnetic resonance imaging (MRI), and so forth.[5−14] In addition, understanding details of nanoscaled magnetic materials in complex core/shell structures is interesting from a fundamental materials science point of view since tailoring their magnetic properties requires understanding of the size effects on the relevant parameters. The accessible range of properties can be greatly extended by mixing different elements and generating intermetallic compounds and alloys. The quest for materials with well-defined, controllable properties and structures on the nanometer scale as well as the flexibility given by intermetallic materials has generated interest in bimetallic and trimetallic nanoclusters, which in the following will be referred to as nanoalloys. In nanoalloys, the chemical and physical properties may be tuned by varying the composition as well as the size of the clusters. They have already been utilized in a number of technologically important areas, ranging from catalysis (e.g., catalytic converters in automobiles and electrochemical fuel cells) to optoelectronic, magnetic, and even medical applications.[15] In particular, the 4d transition metals such as Ru, Rh, and Pd, and the 3d transition metals such as Fe, Co, and Ni and their alloys have been in the focus of both experimental and theoretical investigations. Previous studies have revealed that Ni−Ru alloys could markedly improve the corrosion resistance; however, Ru addition can cause the average magnetic moment of Ni to decrease. The improvement in the corrosion resistance of Ni-based alloys such as Permalloy with a highly soft magnetism is a major precondition for industrial applicability.[16−19] While alloys are indispensable for bulk magnetic applications, improvement of wear resistance upon concomitant tailoring of the magnetic properties as demanded, for example, for nanomedical applications is still a challenging aim for materials synthesis. Hitherto, the synthesis of nanoalloys has been done by using different methods, for example, in the gas phase, in solution, supported on a substrate, or in a matrix.[20] Like other metallocenes, ruthenocene also sublimes and by using an inert carrier gas one can transport and decompose this ruthenocene vapor at high temperatures. In this paper for the first time we report on the synthesis of carbon-coated NiRu nanoalloys by means of the high-pressure chemical vapor deposition method (HPCVD) and we show the effect of the synthesis pressure on the composition, the size, and the magnetic properties of these binary alloys.

2. Experimental Section

2.1. Sample Synthesis. The HPCVD has been applied for the synthesis of carbon-coated NiRu nanoalloys. Here, nickelocene and ruthenocene precursors have been used as sources for the nanoalloying constituents Ni and Ru, respectively. The

* To whom correspondence should be addressed. Fax: +493514659313. E-mail: a.a.m.elgendy@ifw-dresden.de.

10.1021/jp101965x © 2010 American Chemical Society
Published on Web 06/01/2010

TABLE 1: Composition of the NiRu@C Nanostructures Synthesized at Different Pressures As Determined by EDX Analysis[a]

pressure (bar)	13	21	26	31
Ru (wt %)	7.5 ± 0.5	8.3 ± 0.5	19 ± 0.5	16 ± 1
$Ni_{100-x}Ru_x$ (x in wt %)	$Ni_{92.5}Ru_{7.5}$	$Ni_{91.7}Ru_{8.3}$	$Ni_{81}Ru_{19}$	$Ni_{84}Ru_{16}$
C (wt %)	61	73	75	84

[a] The relative amount of carbon has been determined by magnetisation studies (see the text).

setup has been explained in detail before.[21] Briefly, the CVD reactor consists of a quartz tube (48 cm length) placed inside a thick-walled aluminum cylinder with two different temperature zones. The first one (about 30 cm length) is heated to a certain temperature by a Kanthal resistance heater thereby providing the hot zone of the reactor in which the reactions occur due to the thermal decomposition of the metallocenes. The second zone has a temperature that does not exceed 300 °C. This relatively low temperature can be realized by using a water-cooled copper finger inside the quartz tube. The Ni−Ru metallocene powders weight ratio of 2:1 are positioned in a crucible located in a thermostatted chamber at 95 °C and are sublimated and transported using argon gas (1400 sccm) into the reactor. The injection into the reactor is realized by a copper nozzle system through a ceramic insulated water-cooled steel tube. The water cooling is necessary to avoid the metallocene decomposition already outside the reactor. Because of the high flow rate of the carrier gas, the synthesized material transfers from the reaction zone and deposits on the cooling finger surface. In addition to the argon gas (Ar_{cold}) flow inside the quartz tube, the device is equipped with an additional preheated argon inlet (Ar_{hot}) through holes positioned around the nozzle itself. The flow rate of this preheated argon was kept at 140 sccm to mix with the injected cold argon for faster increasing of its temperature inside the reaction zone. For given argon flow rate, it was found that temperature (T) and pressure (P) are crucial to obtain carbon-coated materials. We found that the optimal temperature for the synthesis process amounts to $T = 900$ °C. As will be shown in detail below, changing the pressure affects the amount of Ru inside the alloy as well as the amount of carbon in the whole material.

2.2. Sample Characterization. High-resolution transmission electron microscopy (HRTEM) was realized by means of a FEI Tecnai F 30 TEM with field emission gun at 300 kV. A FEI scanning electron microscope equipped with energy dispersive X-ray (EDX) analysis unit of EDAX has been used using special program for determining the Ru- content inside the nanoalloy. A Miniflex X-ray diffractometer (XRD) with Cu K_α radiation was used to identify the crystal structure. The magnetic field dependence of the magnetization at room temperature was measured by means of a MicroMag Model 2900 (Princeton Measurement Corp.) Alternating Gradient Magnetometer (AGM). The temperature dependence of the magnetization at constant magnetic field in the temperature range 5 to 400 K was studied in a Superconducting Quantum Interference Device (VSM-SQUID) Magnetometer from Quantum Design.

3. Result and Discussion

3.1. Morphology and Structure. The composition of the resulting material was investigated by EDX. In general, our synthesis process yields carbon-coated NiRu nanoalloys (NiRu@C), which actual NiRu ratios depend on the synthesis pressure (see Table 1). For each batch, several EDX measurements were done at different positions of the sample in order to get average values for the core composition. The data imply that moderately increasing the pressure yields a higher Ru content in the sample while at high pressure the composition only very weakly depends on the applied pressure.

The morphology of the coated particles was studied by HRTEM that in general confirms a nanostructured material exhibiting the core/shell structure (Figure 1a). A typical example of NiRu@C is displayed in Figure 1b that shows a spherical NiRu core of about 22 nm and a carbon shell of about 3 nm. We also find carbon-coated nanoalloy particles embedded in a predominantly amorphous carbon matrix (Figure 1c). From the TEM studies, we extracted an average size of the NiRu core of $\langle D_{TEM} \rangle = 8 \pm 3$ nm with a relatively large size distribution as displayed in Figure 1d. The thickness of the carbon shells amounts to 2−3 nm.

A typical XRD diffraction pattern of the deposited material is shown in Figure 2. Noteworthy, we do not observe any characteristic peaks of other related compounds especially oxides. In contrast, the results confirm the pure metallic constitution of the nanoalloy. The diffraction peaks at $2\theta = 39.8$, 44, and 51.5° are related to the main reflexes (100), (002), and (111) of the NiRu alloy that differ from the corresponding reflexes for pure Ni.[18] In contrast, the very broad peak at $2\theta = 26°$ corresponds to graphitic carbon shells and amorphous-like carbon. The XRD pattern also allows the determination of the average diameter of the nanoparticles from the width of the characteristic diffraction peaks. To be specific, we can estimate the average particle size D_{XRD} by applying the Scherrer equation[22]

$$D_{XRD} = \frac{0.93\lambda}{\Delta 2\theta_{(hkl)} \cos \theta_{(hkl)}} \quad (1)$$

Here, λ is the wavelength of the applied Cu Kα radiation, $\Delta 2\theta_{(hkl)}$ is the full width at half-maximum of the diffraction peak, and $\theta_{(hkl)}$ is the Bragg angle. Evaluating the three main reflexes of NiRu (Figure 2) by means of eq 1 yields an average diameter of 6 ± 2 nm, which agrees well with the TEM results. We note that the width of the XRD peaks does not change significantly upon variation of the synthesis pressure, that is, the mean diameters of the metallic cores do not significantly depend on the pressure. In contrast, the peak positions are slightly shifted, which is in agreement with the observed changes in the composition of the nanoalloys.

3.2. Magnetic Properties. The magnetic properties of the prepared samples have been investigated by studies of the field dependence of the magnetization at room temperature and of the temperature dependence at a constant field of $H = 100$ Oe. The field dependencies for the nanoalloys synthesized at various pressure, that is, the full hysteresis loops of the magnetization, in an external field up to 1 T are presented in Figure 3. For the first three samples (13, 21, 26 bar), the data imply a ferromagnetic-like behavior at room temperature, that is, the presence of a remanent magnetization M_r and the saturation of the magnetization curve in rather small external magnetic fields at room temperature. In contrast, at highest pressure a superparamagnetic response is observed. The quantitative analysis of the data reveals a clear dependence of the saturation magnetization on the synthesis pressure (table 2). The comparison with the magnetization of the related bulk NiRu allows estimating the mass ratio of the magnetic material in the carbon-coated particles (Table 1). In general, the saturation magnetization decreases upon increasing the pressure, which is mainly associated with

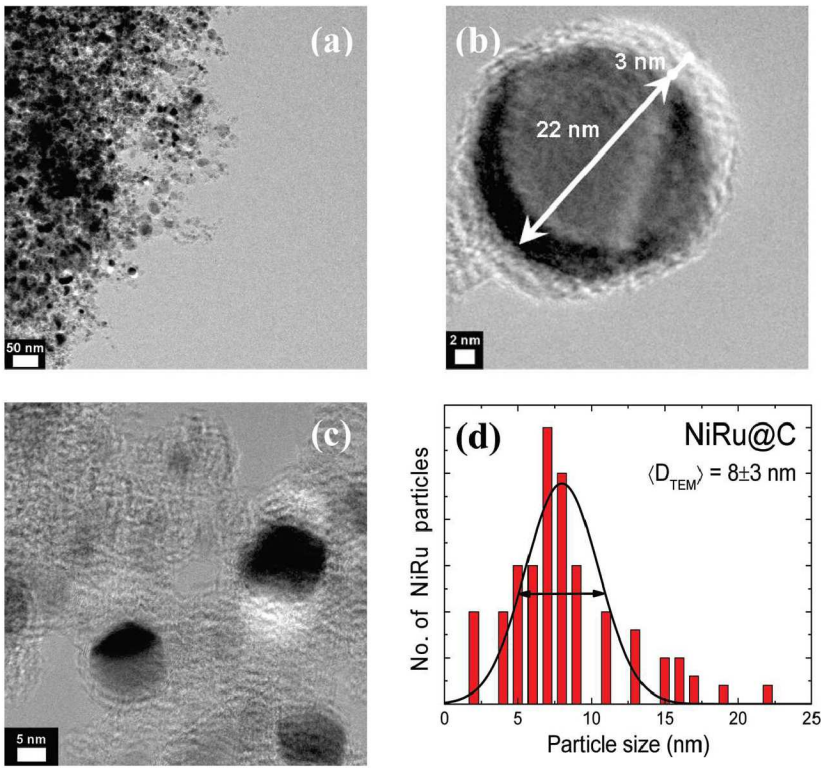

Figure 1. TEM images of (a) NiRu particles coated with carbon shells, (b) example of an individual particle coated with carbon, and (c) carbon-coated NiRu embedded in a predominantly amorphous carbon matrix. (d) Size distribution of the core particles (NiRu). The black line is a Gaussian fit to the data with the HWFM of 3 nm, yielding $\langle D_{TEM} \rangle = 8 \pm 3$ nm.

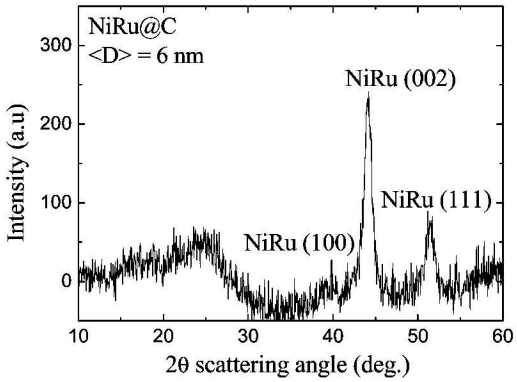

Figure 2. X-ray diffraction spectrum of NiRu@C nanostructures.

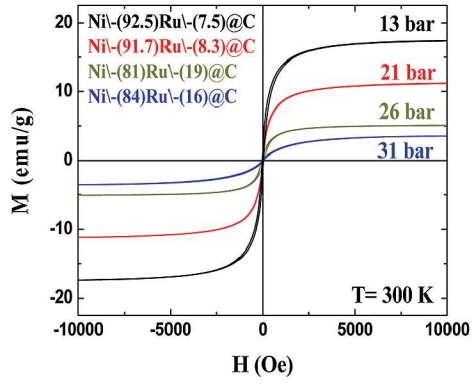

Figure 3. Magnetization loops at room temperature of NiRu@C nanoalloys synthesized at different synthesis pressures.

a decreasing relative amount of magnetic materials, that is, an increase of the relative carbon content. In addition, corresponding to the presence of small spontaneous magnetic moments

TABLE 2: Magnetic Parameters at $T = 300$ K for NiRu@C Synthesised at Different Pressures

pressure (bar)	H_c (Oe)	M_s (emu/g)	M_r (emu/g)	D_{Mag} (NiRu) (nm)	D_{TEM} (NiRu) (nm)	D_{XRD} (NiRu) (nm)
13	30 ± 2	17	1.0 ± 0.1	7.5	8	6
21	6 ± 2	11	0.2 ± 0.1	8.6	9	7
26	45 ± 2	5	0.5 ± 0.1	9.8	9	7
31	26 ± 2	4	0.1 ± 0.1	7.9	8	6

there are small coercive fields H_c close to zero. The other magnetic parameters presented in Table 2 do not show a significant dependence on pressure.

The magnetization studies provide another alternative to deduce information on the size of the magnetic cores by evaluating the initial slopes of the M versus H curves. The major contribution to the initial slope arises from the largest particles. Their larger magnetization vectors are more easily oriented by a magnetic field and thus, an upper boundary for the magnetic size D_{mag} can be estimated by applying eq 2.[23] However, the magnetic field dependence of the magnetization at values near the saturation is determined by the fine particles the orientation of which requires larger fields.

$$D_{mag} = \left[\frac{18 k_B T \frac{(dM)}{(dH)}}{\pi \rho M_s^2} \right]^{1/3} \qquad (2)$$

Here, k_B is the Boltzmann constant, dM/dH is the initial slope near zero field, and ρ is the bulk density of the sample. The analysis of the experimental data in Figure 3 by means of eq 2 hence allows one to estimate an upper boundary for the magnetic core size (cf. Table 2). In agreement with the TEM and XRD

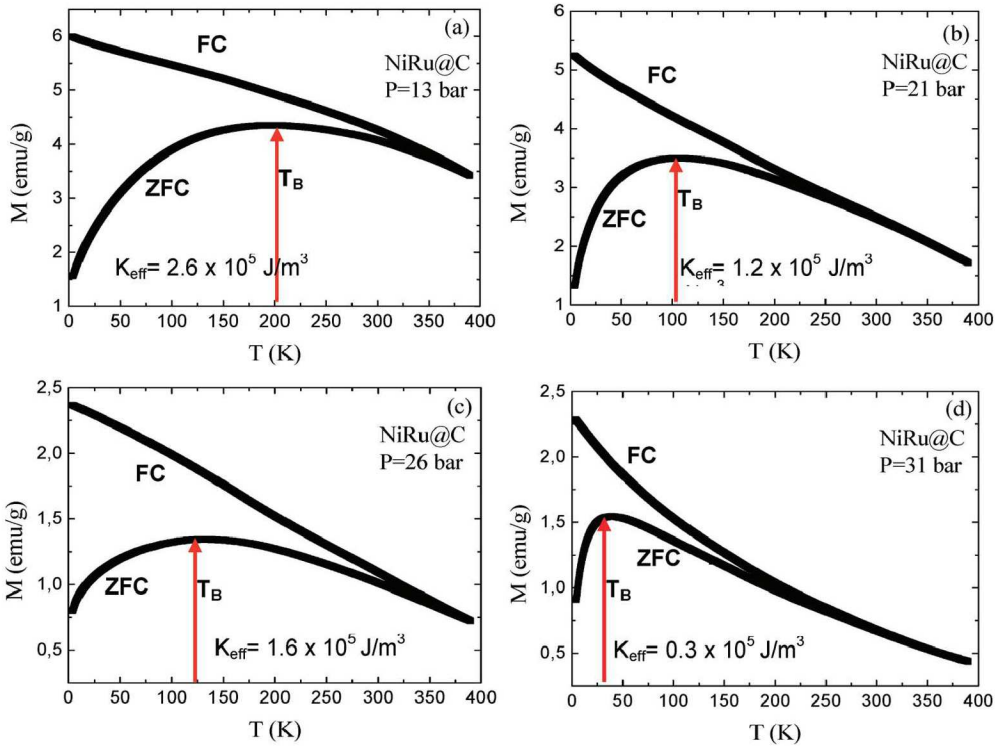

Figure 4. ZFC and FC magnetization curves of NiRu@C nanocapsules at $H = 100$ Oe, prepared at a pressure of (a) 13, (b) 21, (c) 26, and (d) 31 bar, respectively.

analyses, the estimated particle size from the magnetic properties amounts to 8.5 ± 1 nm for all samples under study. The similar core size of all materials is also confirmed by the similar values of the critical field H_c. In contrast, there are strong differences in the saturation magnetization. This value depends both on the relative amount of magnetic core material in the samples and on its composition. Since the composition is known from our EDX analysis, the comparison of the saturation magnetization enables to deduce the nanoalloy to carbon ratio by considering the corresponding values of pure NiRu bulk material.[16] As displayed in Table 1, the relative amount of carbon sensitively depends on the applied synthesis pressure and it monotonously increases at higher pressure. Note that the actual amount of carbon in the samples implies average interparticle distances of 20−30 nm between the particle centers. This yields only small dipolar interactions in the range of a few Kelvin which can be neglected in our analysis of the room temperature magnetization.

The data in Figure 3 imply that, starting from a superparamagnetic behavior at highest pressure, the remanent magnetization at room temperature increases upon lowering the pressure. Superparamagnetic behavior for the material made at 31 bar at 300 K implies that the superparamagnetic blocking temperature of the whole ensemble is smaller than 300 K. This is also seen in Figure 4 where the temperature dependence of the magnetization is shown. In contrast, for the other samples we find finite remanent magnetization at room temperature that indicates that at least a part of the particles exhibit a blocking temperature $T_B > 300$ K. We note that due to the observed size distribution, the superparamagnetic blocking temperatures are supposed to cover a large temperature range for each of the materials. In particular, the smallest particles might exhibit superparamagnetic behavior down to lowest temperatures.

However, the blocking temperature depends not only on the particle size but also on the actual magnetic anisotropy of the material. This is underlined by the fact that the mean diameter of the particles as measured by XRD and TEM is very similar for all materials. To study this in more detail, we hence have measured the temperature dependence of the magnetization for all samples as presented in Figure 4. Here, the samples were first cooled down to 5 K in zero magnetic fields and then a magnetic field of 100 Oe was applied to the samples. Under such 'zero-field-cooled' (ZFC) conditions the measurements were performed upon heating up to 400 K. In contrast, field-cooled (FC) data were obtained after cooling the sample in the same field which was used for the actual measurements.

Figure 4 exhibits a cusp in the zero-field cooled (ZFC) magnetization that might be attributed to the blocking temperature, T_B. However, the ZFC-FC curves depart from each other already at temperatures far beyond the peak in the ZFC curve. On the other hand, the FC magnetization continues to increase without indication of saturation below the peak in the ZFC, which distinguishes the system from the canonical spin-glass systems.[24] The broad size distribution of our nanoparticles already implies a broad distribution of blocking temperatures so that one can attribute the observed ZFC maxima with the blocking temperature of the particles with the mean diameter. In general, for superparamagnetic particles the blocking temperature T_B is linked via the Neel-Brown equation $T_B = K_{eff}V/25k_B$ to the anisotropy energy barrier $K_{eff}V$. Here, K_{eff} is the effective magneto-crystalline anisotropy constant and V is the volume of the magnetic particle.[25,26] By assuming a mean blocking temperature at the ZFC maxima associated with the mean diameter as given above, our data yield anisotropy constants of $2.6-0.3 \times 10^5$ J/m^3 for the four samples presented in Figure 4a−d. On the other hand, the broad size distribution implies that a considerable amount of particles is ferromagnetic at room temperature in which case the coercivity is given by eq 3[27,28]

$$H_C = \frac{2K_{eff}}{M_s}\left[1 - \left(\frac{25K_BT}{K_{eff}V}\right)^{1/2}\right] \quad (3)$$

By knowing the values of H_c, M_s, and the volume of the magnetic particles, our data yield anisotropy constants of $3.8-0.2 \times 10^5$ J/m^3 for the four samples, which is in the same order of the estimated values by using Neel-Brown formula. However, these values are high compared to value to bulk Ni where K_{eff} equals 4.5×10^3 J/m^3. Similar high values of compared to the bulk materials have also been observed for other magnetic nanoparticles and are often ascribed to the surface anisotropy effects of the clusters.[27,29]

4. Conclusion

NiRu@C nanoalloys synthesized by HPCVD have been investigated with respect to their morphology and magnetic properties. Core/shell nanostructures of NiRu@C are formed with a mean core size of 8 nm as derived from the analysis of our HRTEM, XRD, and magnetization data. X-ray diffraction investigation reveals NiRu binary alloys only and no oxidized metals. It is to be particularly mentioned that the content of carbon in the deposited nanoalloy material as well as the actual Ni−Ru ratio clearly depends on the synthesis pressure while the average sizes of the nanoparticles do not significantly change. We can hence control the composition of the produced alloy by controlling the pressure during the synthesis process. This straightforwardly affects the magnetic properties, too. The magnetization curves show ferromagnetic-like behavior at room temperature for the low-pressure samples and typical superparamagnetic behavior for the sample made at highest. Different values for the saturation magnetization are affected by variations in the chemical composition of the NiRu core but primarily caused by different carbon contents in the deposited material, especially by more amorphous-like carbon while the thickness of the graphitic shells is relatively constant. On the other hand, the mean superparamagnetic blocking temperatures are mainly associated with the changing of the chemical composition of the core material. A large anisotropy has been noticed from the analysis of (ZFC) magnetization curve. Because of the particular magnetic properties of NiRu nanoalloy, its uniform coating carbon shells and in particular due to the possible tailoring of the magnetism, the material is a promising candidate for biomedical applications, for example, for magnetic hyperthermia by means of core−shell magnetic nanoparticles and as contrast agent for magnetic resonance imaging.

Acknowledgment. This research was partly supported by the European Community through the Marie Curie Research Training Network CARBIO under contract MRTN-CT-2006-035616, BMBF CARBOMETAL under contract 03 × 0057D and DFG under contract HA5133/4-1. A.A.E. acknowledges funding by the Egyptian government via Grant 2/2/66/2005. Thanks to G. Kreutzer and S. Pichl for technical support at TEM and EDX measurements.

References and Notes

(1) Sounderya, N.; Zhang, Y. Use of Core/Shell Structured Nanoparticles for Biomedical Applications. *Recent Pat. Biomed. Eng.* **2008**, *1*, 34–42.

(2) Liu, X.; Gurel, V.; Morris, D.; Murray, D.; Zhitkovich, A.; Kane, A. B.; Hurt, R. H. Bioavailability of Nickel in Single-Wall Carbon Nanotubes. *Adv. Mater.* **2007**, *19*, 2790–2796.

(3) Guo, L.; Morris, D.; Liu, X.; Vaslet, C.; Hurt, R. H.; Kane, A. B. Iron Bioavailability and Redox Activity in Diverse Carbon Nanotube Samples. *Chem. Mater.* **2007**, *19*, 3472–3478.

(4) Borysiuk, J.; Grabiasa, A.; Szczytkob, J.; Bystrzejewskic, M.; Twardowskib, A.; Lange, H. Structure and magnetic properties of carbon encapsulated Fe nanoparticles obtained by arc plasma and combustion synthesis. *Carbon* **2008**, *46*, 1693–1701.

(5) Kuramochi, H.; Akinaga, H.; Semba, Y.; Kijima, M.; Uzumaki, T.; Yasutake, M.; Tanaka, A.; Yokoyama, H. CoFe-coated carbon nanotube probe for magnetic force microscopy. *Jpn. J. Appl. Phys.* **2005**, *44*, 2077–2080.

(6) Fonseca, F. C.; Ferlauto, A. S.; Alvarez, F.; Goya, G. F.; Jardin, R. F. Morphological and magnetic properties of carbon-nickel nanocomposite thin films. *J. Appl. Phys.* **2005**, *97*, 044313−1−044313−7.

(7) Wang, H.; Wong, S. P.; Cheung, W. Y.; Ke, N.; Chiah, M. F.; Liu, H.; Zhang, X. X. Microstructure evolution, magnetic domain structure, and magnetic properties of Co-C nanocomposite films prepared by pulsed-filtered vacuum arc deposition. *J. Appl. Phys.* **2000**, *88*, 2063–2067.

(8) Delaunay, J. J.; Hayashi, T.; Tomita, M.; Hirono, S.; Umemura, S. CoPt-C nanogranular magnetic thin films. *Appl. Phys. Lett.* **1997**, *71*, 3427–3429.

(9) Vyalikh, A.; Wolter, A.; Hampel, S.; Haase, D.; Ritschel, M.; Leonhardt, A.; Grafe, H.-J.; Taylor, A.; Krämer, K.; Büchner, B.; Klingeler, R. A carbon-wrapped nanoscaled thermometer for temperature control in biological environments. *Nanomedicine* **2008**, *3*, 321–327.

(10) Taylor, A.; Kraemer, K.; Hampel, S.; Fuessel, S.; Klingeler, R.; Ritschel, M.; Büchner, B.; Grimm, M.-O.; Wirth, M. P. Carbon coated nanomagnets as potential hyperthermia agents. *J. Urology* **2008**, *179*, 392–393.

(11) Klingeler, R.; Hampel, S.; Büchner, B. Carbon nanotube based biomedical agents for heating, temperature sensoring and drug delivery. *Int. J. Hyperthermia* **2008**, *24*, 496–505.

(12) Jordan, A.; Scholz, R.; Wust, P.; Fahling, H.; Felix, R. Magnetic fluid hyperthermia (MFH): Cancer treatment with AC magnetic field induced excitation of biocompatible superparamagnetic nanoparticles. *J. Magn. Magn. Mater.* **1999**, *201*, 413–419.

(13) Johannsen, M.; Gneveckow, U.; Taymoorian, K.; Thiesen, B.; Waldöfner, N.; Scholz, R.; Jung, K.; Jordon, A.; Wust, P.; Loening, S. A. Morbidity and quality of life during thermotherapy using magnetic nanoparticles in locally recurrent prostate cancer: Results of a prospective phase I trial. *Int. J. Hyperthermia* **2007**, *23*, 315–323.

(14) Krupskaya, Y.; Mahn, C.; Parameswaran, A.; Taylor, A.; Kraemer, K.; Hampel, S.; Leonhardt, A.; Ritschel, M.; Büchner, B.; Klingeler, R. Magnetic study of iron-containing carbon nanotubes: Feasibility for magnetic hyperthermia. *J. Magn. Magn. Mater.* **2009**, *321*, 4067–4071.

(15) Robinson, I.; Zacchini, S.; Tung, L. D.; Maenosono, S.; Thanh, N. T. K. Synthesis and Characterization of Magnetic Nanoalloys from Bimetallic Carbonyl Clusters. *Chem. Mater.* **2009**, *21*, 3021–3026.

(16) Crangle, J.; Parsons, D. The magnetization of ferromagnetic binary alloys of cobalt or nickel with elements of the palladium and platinum groups. *Proc. R. Soc. London, Ser. A* **1960**, *255*, 509–519.

(17) Armigliatoa, A.; Bigib, S.; Moggic, P.; Papadopulosc, S.; Predieri, G.; Salviatid, G.; Sappa, E. Production of Ni-Ru bimetallic catalysts and materials by thermal and chemical decomposition of a tetranuclear bimetallic carbonyl cluster. *Mater. Chem. Phys.* **1991**, *29*, 251–260.

(18) Deng, S.; Pingali, K. C.; Rockstraw, D. A. Synthesis of Ru-Ni Core-Shell Nanoparticles for Potential Sensor Applications. *IEEE Sensor J.* **2008**, *8* (6), 730–734.

(19) Crisafulli, C.; Scirè, S.; Minicò, S.; Solarino, L. Ni-Ru bimetallic catalysts for the CO2 reforming of methane. *Appl.Catal., A.* **2002**, *225*, 1–9.

(20) Ferrando, R.; Jellinek, J.; Johnston, R. L. Nanoalloys: From Theory to applications of Alloy Clusters and Nanoparticles. *Chem. Rev.* **2008**, *108*, 845–910.

(21) El-Gendy, A. A.; Ibrahim, E. M. M.; Khavrus, V. O.; Krupskaya, Y.; Hampel, S.; Leonhardt, A.; Büchner, B.; Klingeler, R. The synthesis of carbon coated Fe, Co and Ni nanoparticles and an examination of their magnetic properties. *Carbon* **2009**, *47*, 2821–2828.

(22) Patterson, A. L. The Scherrer formula for X-Ray particle size determination. *Phys. Rev. Lett.* **1939**, *56*, 978–982.

(23) Glaspell, G.; Abdelsayed, V.; Saoud, K. M.; El-Shall, M. S. Vapor-phase synthesis of metallic and intermetallic nanoparticles and nanowires: Magnetic and catalytic properties. *Pure Appl. Chem.* **2006**, *78*, 1667–1689.

(24) Binder, K.; Young, A. P. Spin glasses: Experimental facts, theoretical concepts, and open questions. *Rev. Mod. Phys.* **1986**, *58*, 801–976.

(25) Borysiuk, J.; Grabiasa, A.; Szczytkob, J.; Bystrzejewskic, M.; Twardowskib, A.; Lange, H. Structure and magnetic properties of carbon encapsulated Fe nanoparticles obtained by arc plasma and combustion synthesis. *Carbon* **2008**, *46*, 1693–1701.

(26) Zhang, X. X.; Hernandez, J. M.; Tejada, J.; Sole, R.; Ruiz, X. Magnetic properties and domain-wall motion in single-crystal BaFe10.2Sn0.74Co0.66O19. *Phys. Rev. B* **1996**, *53*, 3336–3340.

(27) Peng, a.; D, L.; Chena, Y.; Shea, H.; Katoh, R.; Sumiyama, K. Preparation and magnetic characteristics of size-monodispersed Fe-Co alloy cluster assemblies. *J. Alloys Compd.* **2009**, *469*, 276–281.

(28) Cullity, B. D. *Introduction to Magnetic Materials*; Addison-Wesley: London, 1972; p 415, 417.

(29) Ammar, S.; Helfen, A.; Jouini, N.; Fievet, F.; Rosenman, I.; Villain, F.; Molinie, P.; Danot, M. Magnetic properties of ultraone cobalt ferrite particles synthesized by hydrolysis in a polyol medium. *J. Mater. Chem.* **2001**, *11*, 186–192.

JP101965X